

Recursive Fermi-operator expansion strategies to accelerate subspace diagonalization for large eigenvalue problems in density functional theory

Sameer Khadatkar¹ and Phani Motamarri¹
Indian Institute of Science, Bengaluru, India.

(*Electronic mail: phanim@iisc.ac.in)

Quantum mechanical calculations for material modelling using Kohn-Sham density functional theory (DFT) involve the solution of a nonlinear eigenvalue problem for N smallest eigenvector-eigenvalue pairs with N proportional to the number of electrons in the material system. These calculations are computationally demanding and have asymptotic cubic scaling complexity with the number of electrons. Large-scale matrix eigenvalue problems arising from the discretization of the Kohn-Sham DFT equations employing a systematically convergent basis traditionally rely on iterative orthogonal projection methods, which are shown to be computationally efficient and scalable on massively parallel computing architectures. However, as the size of the material system increases, these methods are known to incur dominant computational costs through the Rayleigh-Ritz projection step of the discretized Kohn-Sham Hamiltonian matrix and the subsequent subspace diagonalization of the projected matrix. In this work, we explore scalable polynomial expansion approaches based on recursive Fermi-operator expansion using mixed-precision arithmetic as an alternative to the subspace diagonalization of the projected Hamiltonian matrix to reduce the computational cost. We perform a detailed comparison of these polynomial expansion approaches to the traditional approach of explicit diagonalization, utilizing state-of-the-art ELPA library on both multi-node CPU and GPU architectures, and assess their relative performance in terms of accuracy, computational efficiency, scaling behaviour and energy efficiency.

I. INTRODUCTION

Eigenvalue problems are frequently encountered in many scientific disciplines. For instance, the accurate and efficient computation of eigenvectors and eigenvalues is critical in the study of resonance, understanding the stability of fluid flows subjected to small perturbations, obtaining insights into vibrational modes of lattices, dimensionality reduction, and many more. Another well-known and challenging application of eigenvalue problems is in the area of quantum modeling of materials using Kohn-Sham density functional theory (DFT)¹, which has been immensely successful in providing critical insights into various ground-state material properties. To compute the ground-state electronic structure in DFT, one is confronted with solving a large-scale nonlinear eigenvalue problem using a self-consistent field iteration procedure (SCF) for N smallest eigenvalue/eigenvector pairs, with N being proportional to the number of electrons in the material system. This results in asymptotic cubic complexity $\mathcal{O}(N^3)$ with the number of electrons for DFT, making these calculations computationally demanding and often restrictive in terms of system sizes that can be handled using widely used DFT codes. Many of these codes employ plane-wave basis sets, which restrict simulation domains to periodic or atomic-orbital type basis sets, which are not systematically convergent, and these basis sets are not amenable for massive parallelization on parallel computing architectures. To extend the range of system sizes to be studied, numerous past efforts have focused on developing systematically convergent real-space computational methodologies²⁻⁶ that have focused on reducing the prefactor associated with the cubic computational complexity alongside improving the parallel scalability, thereby enabling large-scale DFT calculations up to 100,000 electrons. These real-space DFT discretization approaches result in large sparse Hermitian eigenvalue problems of the form $\mathbf{H}\psi_i = \epsilon_i^h \psi_i$ to be solved for N smallest eigenvalue/eigenvector pairs, with N being proportional to M , the dimension of the sparse Hamil-

tonian matrix \mathbf{H} ($M \approx 10^5 - 10^7$). We note that N depends on the number of electrons in the material system and is usually 0.1 – 0.5% of M , the degrees of freedom (DoFs) used in the simulation.

In the electronic structure community, the most popular eigensolver strategies employed to solve these large DFT eigenvalue problems include the Davidson approach, Locally Optimal Block Pre-conditioned Conjugate Gradient (LOBPCG) method, or the Chebyshev filtered subspace iteration (ChFSI) approach. These eigensolvers belong to the category of iterative orthogonal projection methods (IOP) wherein the matrix \mathbf{H} is orthogonally projected onto a carefully constructed subspace rich in the wanted eigenvectors (Rayleigh-Ritz step), and subsequently, the resulting smaller dense projected Hamiltonian \mathbf{H}^p is explicitly diagonalized (subspace diagonalization) to approximate the desired eigenvalue/eigenvector pairs of the \mathbf{H} matrix. The cubic scaling computational cost of this subspace diagonalization step dominates for medium to large-scale material systems ($N > 20,000$) in comparison to the costs associated with subspace construction and Rayleigh-Ritz steps in IOP methods. For instance, the authors⁶ employing the ChFSI approach have reported that the subspace diagonalization constitutes roughly 30% of the total ChFSI cost for $N \approx 30,000$, whereas it accounts for around 56% of the total cost for $N \approx 50,000$. To this end, the current work explores recursive polynomial expansion approaches based on Fermi-operator expansion as an alternative to the subspace diagonalization procedure to improve the computational efficiency, thereby reducing the computational prefactor associated with the cubic complexity of the subspace diagonalization approach. Furthermore, the energy efficiency and parallel scaling efficiency of these approaches is examined on both multinode CPUs and multinode GPUs.

Recursive polynomial expansion approaches (RPE) rely on the key idea that constructing a density matrix (projec-

tor matrix corresponding to N smallest eigenvectors) suffices to compute ground-state electronic structure in DFT at zero-temperature without the necessity of knowing explicit eigenvalues and eigenvectors. These RPE approaches^{7–12} have been explored in the past for conducting ground-state DFT calculations using atomic-orbital basis. However, the computational efficiency, scaling and energy efficiency of these approaches have not been explored in comparison to subspace diagonalization procedures for their use in iteration orthogonal projection methods on multinode CPU and GPU architectures. The evolving computing architectures in today’s exascale era place a heavy emphasis on scalable methodologies with a focus on reduced data movement and increased arithmetic intensity, with an equal emphasis on using energy-efficient algorithms. The current work assumes significance in this regard and is useful for solving large-scale eigenvalue problems arising from the discretization of DFT using systematically convergent basis sets employing IOP methods. To this end, the key contributions of our current work, as described in the subsequent sections, include – (a) efficient implementation strategies of various recursive polynomial expansion (RPE) techniques based on Fermi-operator expansion on both multinode CPU and GPU architectures for both zero-temperature case and the finite-temperature case of Fermi-dirac smearing of the occupancy function (b) design of mixed precision strategies in conjunction with RPE to reduce compute and data access costs (c) assessing accuracy, scaling efficiency and energy efficiency of the proposed implementation procedures by comparing it with explicit diagonalization algorithms provided by state-of-the-art ELPA library¹³.

II. RELATED WORK AND BACKGROUND

This section discusses key ideas central to recursive polynomial expansion approaches which are used to approximate the density matrix.

A. Density matrix

At zero electronic temperature, the density matrix (\mathbf{D}) can be defined as a projector matrix corresponding to the lowest occupied ($N_{occ} \leq N$) eigenvectors of the Kohn-Sham Hamiltonian \mathbf{H} matrix. Mathematically, it takes the form of a shifted Heaviside step function, $\theta(\cdot)$, given by $\mathbf{D} = \theta[\mu\mathbf{I} - \mathbf{H}]$. The density matrix (\mathbf{D}) in the case of finite-temperature is a smeared version of zero-temperature density matrix and mathematically represented by a Fermi-operator matrix function given by $\mathbf{D} = [e^{\beta(\mathbf{H} - \mu\mathbf{I})} + \mathbf{I}]^{-1}$, where, \mathbf{I} denotes the identity matrix, $\beta = 1/(k_B T_e)$ is the inverse electronic temperature, μ is the Fermi-energy, and \mathbf{H} is the Hamiltonian matrix. Note that the eigenvalues f_i of \mathbf{D} are referred to as occupancies. f_i is either 0 or 1 for a zero-temperature case whereas for the case of a finite-temperature case, $f_i \in [0, 1]$.

B. Recursive polynomial expansion techniques to approximate the density matrix

Two types of polynomial expansion schemes can be used to approximate the density matrix – (a) Serial Fermi-operator expansion schemes (Chebyshev Fermi-operator expansion

scheme¹⁴, Green’s function expansion scheme¹⁵, etc), (b) Recursive Fermi-operator expansion schemes^{8–12}. In this work, we employ the latter approach i.e., the recursive Fermi-operator expansion schemes as they are shown to be more efficient and can be used to approximate the density matrix for both zero-temperature, and finite-temperature cases as well.

1. Recursive Fermi-operator expansion for zero-temperature density matrix (Z-RFOE)

The recursive Fermi-operator expansion⁸ involves successive projections of a matrix \mathbf{X}_n , where $\mathbf{X}_0 = \mathbf{H}$ and $\mathbf{X}_{n+1} = F(\mathbf{X}_n)$. The functions $F(\mathbf{X}_n)$ are chosen to project the eigenvalue spectrum of \mathbf{X}_n to eigenvalues closer either to 1 or to 0. Mathematically this can be represented as

$$\mathbf{D} = \theta(\mu\mathbf{I} - \mathbf{H}) \approx F_m(F_{m-1}(\dots F_0(\mathbf{H})\dots)) \quad (1)$$

One of the most efficient techniques in Z-RFOE is to use the second-order projection polynomials (SP2)⁹ given by $\mathbf{X}_{n+1} = F_n(\mathbf{X}_n) = \mathbf{X}_n \pm (\mathbf{X}_n - \mathbf{X}_n^2)$. The SP2 here are continuously increasing and decreasing functions in the interval $[0, 1]$. The \pm sign is chosen to adjust the trace of \mathbf{X}_{n+1} in each projection such that it converges to N_{occ} .

2. Accelerated recursive polynomial expansion for zero-temperature density matrix (A-Z-RFOE)

This technique works on the concept of shifting and scaling. In Z-RFOE, we used SP2 polynomials, which either took the form $F(\mathbf{X}) = \mathbf{X}^2$ or $F(\mathbf{X}) = 2\mathbf{X} - \mathbf{X}^2$. In A-Z-RFOE, instead of restricting ourselves to these fixed expansion functions, we give it some freedom to choose the expansion functions such that it moves the eigenvalues closer to either 1 or 0 faster. To optimize the convergence, we chose the polynomial such that each iteration gives the highest slope of projection around the eigenvalues, which are rescaled values of the HOMO (Highest Occupied Molecular Orbital) and LUMO (Lowest Unoccupied Molecular Orbital) eigenvalues and done such that there is no risk of eigenvalues switching the places between the occupied and the unoccupied states¹⁰.

3. Recursive Fermi-operator expansion scheme for finite-temperature cases (T-RFOE)

Finite-temperature density matrix has occupancies $f_i \in [0, 1]$ and the SP2 recursion scheme discussed above is not well suited for approximating density matrix with fractional occupancies. To this end, an intermediate function generated in Z-RFOE that is obtained before the convergence of the algorithm to the projector matrix is used. This serves as a smeared function to zero-temperature density matrix (Heaviside step function). To this end, the truncated expansion for computing, the density matrix \mathbf{D} can be given by the expression in (2).

$$G_m(\mathbf{H}) = F_m(F_{m-1}(\dots F_0(\mathbf{H})\dots)) \quad (2)$$

Lower the electronic temperature T_e higher will be the β value (refer to Sec. IIA), and more recursion steps m will be required to approximate the density matrix^{11,12}.

C. Accuracy of the polynomial expansion procedures

The accuracy of the aforementioned polynomial expansion procedures is given in terms of the degree n_{pl} of the polynomial needed to approximate the density matrix and is given by $n_{pl} \propto (\epsilon_N - \epsilon_1)$ with ϵ_1, ϵ_N being spectral bound estimates of \mathbf{H}^{16} . It is well known that DFT discretized Hamiltonian \mathbf{H} using real-space approaches has large spectral width $\epsilon_N - \epsilon_1$ resulting in higher n_{pl} for approximating the density matrix. Often this leads to an inefficient computational procedure to approximate the density matrix since the dimension of \mathbf{H} can be of $\mathcal{O}(10^5 - 10^7)$.

III. COMPUTATIONAL METHODOLOGY AND IMPLEMENTATION

A. Proposed methodology

Due to the aforementioned limitations of employing the recursive polynomial expansion procedures on the real-space discretized DFT Hamiltonian (\mathbf{H}), we resort to iterative orthogonal projection (IOP) methods of solving a large sparse eigenvalue problem and choose to work with the smaller dense projected Hamiltonian \mathbf{H}^p in the subspace rich with eigenvectors of \mathbf{H} . To this end, we employ the recursive polynomial expansion procedures on \mathbf{H}^p to approximate the density matrix in the subspace as an alternative to explicit subspace diagonalization. Since the spectral width of \mathbf{H}^p is commensurate with spectral width corresponding to occupied eigenstates, it is small and the proposed approach is computationally efficient as demonstrated subsequently.

B. Algorithmic details

Using \mathbf{H}^p , Z-RFOE and A-Z-RFOE schemes employing SP2 polynomials for approximating zero-temperature density matrix and the T-RFOE scheme for the finite-temperature density matrix have been implemented in a distributed setting. Figure 1 shows the schematic of the RFOE algorithm implemented in the current work.

Furthermore, we also explored mixed-precision strategies in conjunction with the RFOE schemes implemented in this work. To this end, we rely on the fact that far away from RFOE convergence to the appropriate density matrix, the floating point operations involved in the initial RFOE iterations can be performed in single precision (FP32) and switching to FP64 operations thereafter. The criteria to decide the number of initial FP32 iterations is linked to relative trace change of \mathbf{X}_n (ϵ_{tr}) of two successive RFOE iterations. An estimate of ϵ_{tr} could be obtained by examining the dependence of ϵ_{tr} on the relative change in occupied eigensubspace between the starting matrix $\mathbf{X}_0 = \mathbf{H}^p$ and the intermediate matrices \mathbf{X}_n generated during the course of RFOE. Our numerical studies on smaller size representative \mathbf{H}^p arising in DFT show that $\epsilon_{tr} \approx \mathcal{O}(10^{-4})$ gives an acceptable error of $\mathcal{O}(10^{-7})$ with respect to fully double precision (FP64) computation of the density matrix.

C. Implementation details

The multinode parallel implementation of RFOE codes was done in C++ employing Message Passing Interface (MPI) library. Software for Linear Algebra Targeting Exascale (SLATE) library¹⁷ was used for storing the parallel matrices encountered during the course of RFOE. SLATE stores the matrix in a 2-D block-cyclic manner on both CPUs and GPUs within a node. The tile size is the most basic parameter that can affect the SLATE routines' performance. Numerical experiments were conducted by varying the tile size to decide the optimal tile size.

Some of the key aspects of the implementation are highlighted below:

1. Trace Calculations

Traces of matrix squares are required during the course of RFOE iterations and are computed by evaluating the square of the Frobenius norm of the given symmetric matrix ($Tr(A^2) = \|A\|_F^2$). To this end, Frobenius norm function available in the SLATE library was used. Further, the computations of matrix traces which was required only in the beginning and end of RFOE involved a traversal through the diagonal elements of the global matrix and the use of an MPI collective function.

2. Matrix-matrix multiplication

The computationally dominant step in all the RFOE algorithms implemented is the matrix-matrix multiplication step. We used the SLATE library functions to perform this step in parallel across multinode CPUs and GPUs. The performance of the Communication-optimal Matrix Multiplication (COSMA)¹⁸ and cuBLASmG (made available from CUDA Math Library Early Access Program¹⁹) library was also explored to compute parallel matrix-matrix multiplications on CPUs and GPUs. Our studies indicates that COSMA was slower in terms of computational times compared to the SLATE library. And the cuBLASmG library is restricted to multi-GPUs within a single node.

D. Metrics for accuracy benchmarking of RFOE

For accuracy benchmarking of the RFOE methods implemented, we computed two errors: (a) Relative error between the exact and approximated density matrix ($f(\mathbf{H})$) using the Frobenius norm, i.e $\epsilon_1 = (\|\mathbf{D} - \mathbf{D}_{ref}\|_F) / \|\mathbf{D}_{ref}\|_F$, (b) Relative error between the trace of actual and the approximated $f(\mathbf{H})\mathbf{H}$, $\epsilon_2 = (tr(\mathbf{D}\mathbf{H}) - tr(\mathbf{D}_{ref}\mathbf{H})) / tr(\mathbf{D}_{ref}\mathbf{H})$. \mathbf{D}_{ref} was computed by explicit diagonalization using ELPA library¹³.

IV. RESULTS AND DISCUSSION

In order to assess the accuracy and performance of the proposed methods, we employ synthetic matrices representative of the subspace projected Hamiltonians (\mathbf{H}^p) arising in DFT calculations. To this end, the matrix \mathbf{H}^p is constructed in such a way that the spectral width is smaller and remains constant with increase in matrix size. We choose $H_{ij}^p = H_{ji}^p =$

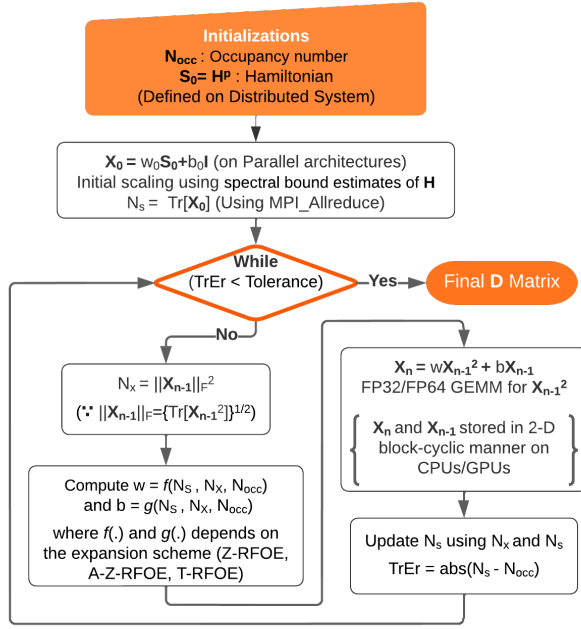


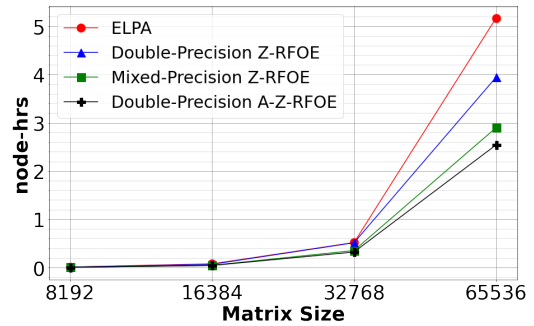
FIG. 1: General implementation details flowchart for all the RFOE codes

$e^{-d*|i-j|} * \sin(i+1)$, and the matrix sizes used were 8192×8192 , 16384×16384 , 32768×32768 , and 65536×65536 . The multinode CPU study was done on PARAM Pravega having Intel Xeon Cascade Lake 8268 CPU (2.9 GHz) with 48 cores (96 threads) on each node, while multinode GPU study was done on a local lab cluster having 16x (8 on each node) NVIDIA Tesla V100 GPUs with 32 GB of memory. The performance metrics used for comparisons are:

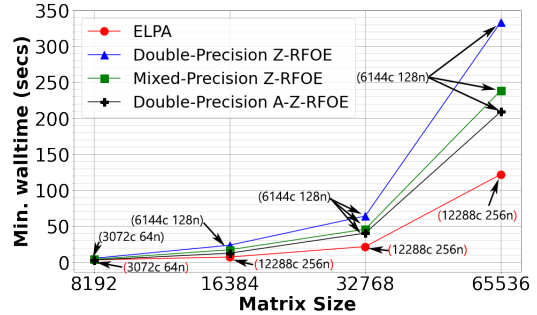
- Node-hrs \Rightarrow Execution time (in hours) \times the number of nodes taken in the best scaling regime. It gives a measure of computational efficiency on CPUs.
- GPU-hrs \Rightarrow Execution time (in hours) \times the number of GPUs taken in the best scaling regime. It gives a measure of computational efficiency on GPUs.
- Minimum walltime \Rightarrow Least possible time for the job execution using as many resources as possible. It is a measure of scaling efficiency of the implementation.
- Energy consumption \Rightarrow Upper bound of the energy required by the job in kWh to run it on the supercomputer. Indicative of the rupee cost required for the calculations on the supercomputer. For the energy consumption calculation we used the Thermal Design Power (TDP) ratings for both CPUs and GPUs.

1. Multinode CPU comparisons

Figure 2 shows that, all our RFOE implementations for zero-temperature case are better than ELPA in terms of node-



(a)



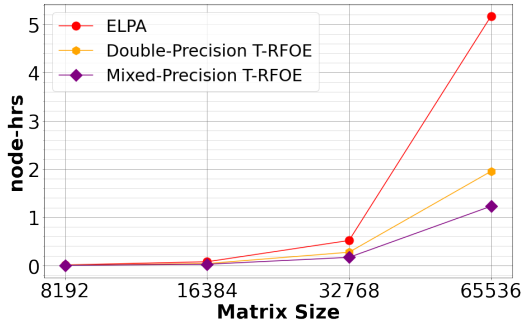
(b)

FIG. 2: (a) Node-hrs vs. matrix size plot, and (b) Min. walltime vs. matrix size plot (Note: c stands for CPUs, n stands for nodes) for different implementations of RFOEs for zero-temperature case on multinode CPUs.

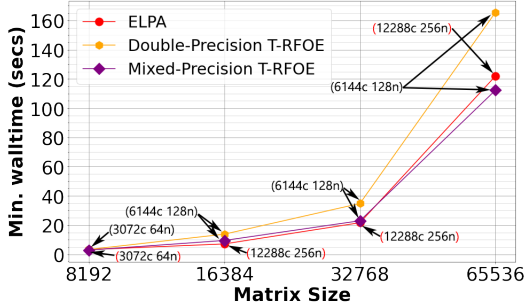
hrs, which indicates that all of our implementations are computationally efficient compared to ELPA. For instance, the A-Z-RFOE results in a speedup of around 2x in comparison to ELPA for the 65536 size matrix. In the minimum walltime regime, we find that ELPA is slightly faster than the RFOE implementation for the matrix sizes considered. Figure 3 shows that, both our T-RFOE and mixed-precision T-RFOE implementations for finite-temperature case are better than ELPA in terms of node-hrs (4.2x speedup of mixed-precision T-RFOE implementation over ELPA for the 65536 size matrix), which indicates that both of our implementations are computationally efficient compared to ELPA. And, even in the minimum walltime, mixed precision T-RFOE was found to be slightly better than ELPA. The number of CPUs on which we got minimum walltime for different matrix sizes is also shown on the minimum walltime plots.

2. Multinode GPU comparisons

Figure 4 shows that, all our implementations for zero-temperature case are better than ELPA up to 16384 size matrix, and beyond this size, the mixed-precision Z-RFOE and A-Z-RFOE are better than ELPA for GPU-hrs timings, which indicates that both of our implementations are computationally efficient compared to ELPA. Our A-Z-RFOE implementation gave 1.5x speedup over ELPA for the 32768 size matrix. Due to the memory issue of ELPA, it does not work on multinode GPUs up to 16 GPUs for the 65536 size ma-



(a)



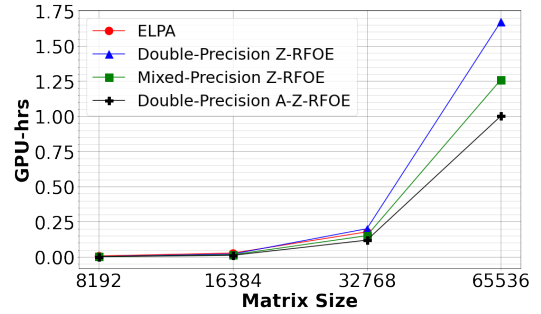
(b)

FIG. 3: (a) Node-hrs vs. matrix size plot, and (b) Min. walltime vs. matrix size plot (Note: c stands for CPUs, n stands for nodes) for different implementations of RFOEs for finite-temperature case on multinode CPUs.

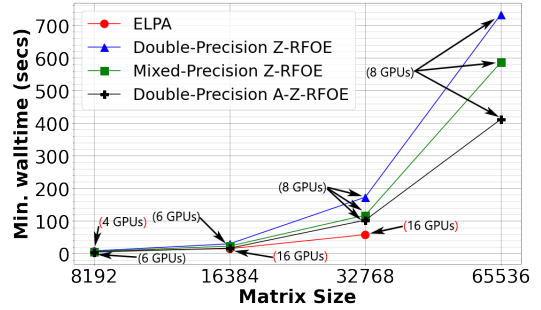
trix, which indicates that the RFOE implementations use the memory efficiently compared to ELPA. And for minimum walltime, ELPA shows a better behaviour, suggesting that the RFOE implementations are not scaling well on multinode GPUs. Figure 5 shows that, our T-RFOE and mixed-precision T-RFOE implementations for finite-temperature case are better than ELPA for GPU-hrs timings (2.5x speedup of mixed-precision T-RFOE implementation over ELPA for the 65536 size matrix), indicating that both implementations are computationally efficient compared to ELPA. And, for minimum walltime, our mixed-precision T-RFOE implementation is almost similar to or better than ELPA. The number of GPUs on which we got minimum walltime for different matrix sizes is shown on the minimum walltime plot.

3. Energy consumption comparisons

Figure 6 shows that, in both the regimes of node-hrs/GPU-hrs and minimum walltime, we are better than ELPA in terms of energy consumption for zero-temperature case. Figure 7 shows that, in both the regimes of node-hrs/GPU-hrs and minimum walltime case, we are better than ELPA in terms of energy consumption for finite-temperature case. This indicates that the rupee cost required for our calculations on the super-computer will be less than ELPA for both zero-temperature case and finite-temperature case of approximating the density matrix.

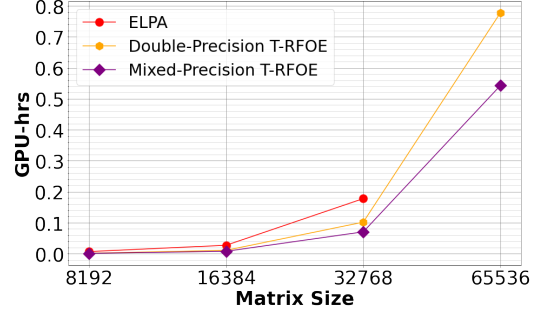


(a)

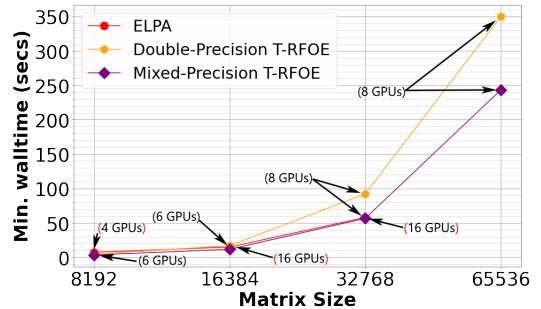


(b)

FIG. 4: (a) GPU-hrs vs. matrix size plot, and (b) Min. walltime vs. matrix size plot for different implementations of RFOEs for zero-temperature case on multinode GPUs.

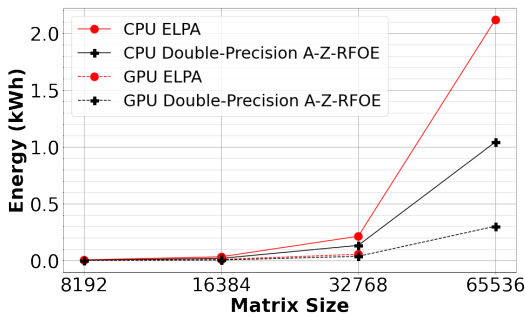


(a)

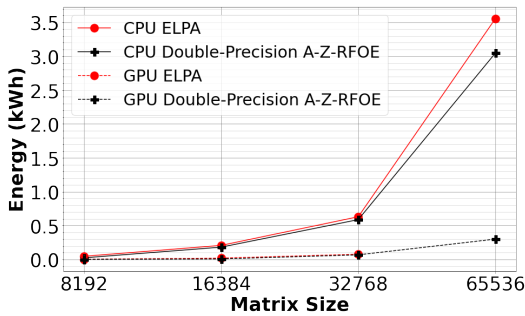


(b)

FIG. 5: (a) GPU-hrs vs. matrix size plot, and (b) Min. walltime vs. matrix size plot for different implementations of RFOEs for finite-temperature case on multinode GPUs.

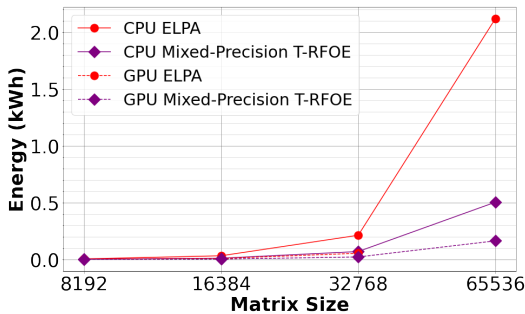


(a)

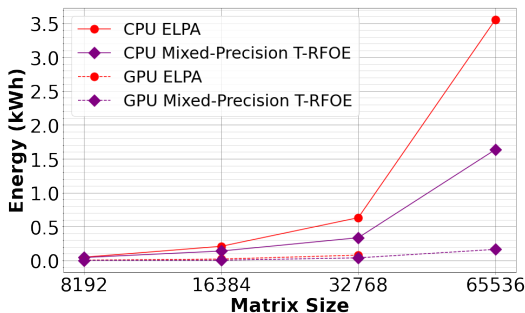


(b)

FIG. 6: Energy consumption (kWh) vs. matrix size plot in terms of (a) Node-hrs/GPU-hrs, and (b) Min. walltime for the best implementation of RFOE for zero-temperature case.



(a)



(b)

FIG. 7: Energy consumption (kWh) vs. matrix size plot in terms of (a) Node-hrs/GPU-hrs, and (b) Min. walltime for the best implementation of RFOE for finite-temperature case.

4. Accuracy benchmarking

The errors ϵ_1 and ϵ_2 (defined earlier) were of the $O(10^{-10})$ and $O(10^{-09})$ for double-precision implementation of Z-RFOE and A-Z-RFOE. And, were of the $O(10^{-07})$ and $O(10^{-09})$ for mixed-precision implementation of Z-RFOE.

For T-RFOE, the error ϵ_1 was of the $O(10^{-03})$ and ϵ_2 was of $O(10^{-06})$. The density matrix approximated by T-RFOE has a higher error compared to the Fermi-Dirac based density matrix. However, in DFT, the computation of material properties relies on differences in energies and hence, the T-RFOE approach can be viewed as an alternative approach to smearing the zero-temperature density matrix, which can be practically helpful in approximating finite-temperature density matrix.

V. CONCLUSIONS

RFOE schemes, as expected, had a lesser computational prefactor which made them computationally efficient compared to ELPA in the node-hrs/GPU-hrs regime. In the case of minimum walltimings, ELPA timings were better as it scaled better than our RFOE implementations. Energy efficiency-wise, the RFOE implementations were better on both multinode CPUs and GPUs, which is directly proportional to the cost required for the computations. In terms of memory utilization, multinode GPU implementations of RFOE were better than ELPA. From all the observations we can conclude that, these techniques can be used whenever we have fewer computational resources and have cost constraints.

¹W. Kohn and L. J. Sham, “Self-consistent equations including exchange and correlation effects,” *Phys. Rev.* **140**, A1133–A1138 (1965).

²L. E. Ratcliff, W. Dawson, G. Fiscaro, D. Caliste, S. Mohr, A. Degomme, B. Videau, V. Cristiglio, M. Stella, M. D’Alessandro, S. Goedecker, T. Nakajima, T. Deutsch, and L. Genovese, “Flexibilities of wavelets as a computational basis set for large-scale electronic structure calculations,” *The Journal of Chemical Physics* **152**, 194110 (2020).

³S. Ghosh and P. Suryanarayana, “SPARC: Accurate and efficient finite-difference formulation and parallel implementation of density functional theory: Isolated clusters,” *Computer Physics Communications* **212**, 189–204 (2017).

⁴S. Das, P. Motamarri, V. Gavini, B. Turcksin, Y. W. Li, and B. Leback, “Fast, scalable and accurate finite-element based ab initio calculations using mixed precision computing: 46 pflops simulation of a metallic dislocation system,” in *Proc. of the International Conference for High Performance Computing, Networking, Storage and Analysis* (2019).

⁵P. Motamarri, S. Das, S. Rudraraju, K. Ghosh, D. Davydov, and V. Gavini, “DFT-FE – a massively parallel adaptive finite-element code for large-scale density functional theory calculations,” *Computer Physics Communications* **246**, 106853 (2020).

⁶S. Das, P. Motamarri, V. Subramanian, D. M. Rogers, and V. Gavini, “DFT-FE 1.0: A massively parallel hybrid cpu-gpu density functional theory code using finite-element discretization,” (2022).

⁷J. Finkelstein, J. S. Smith, S. M. Mniszewski, K. Barros, C. F. A. Negre, E. H. Rubensson, and A. M. N. Niklasson, “Mixed precision fermi-operator expansion on tensor cores from a machine learning perspective,” *Journal of Chemical Theory and Computation* **17**, 2256–2265 (2021).

⁸A. M. N. Niklasson, “Expansion algorithm for the density matrix,” *Phys. Rev. B* **66**, 155115 (2002).

⁹G. Beylkin, N. Coult, and M. J. Mohlenkamp, “Fast spectral projection algorithms for density-matrix computations,” *Journal of Computational Physics* **152**, 32–54 (1999).

¹⁰E. H. Rubensson and A. M. N. Niklasson, “Accelerated density matrix expansions for born-oppenheimer molecular dynamics,” (2013).

- ¹¹S. M. Mniszewski, R. Perriot, E. H. Rubensson, C. F. A. Negre, M. J. Cawkwell, and A. M. N. Niklasson, “Linear scaling pseudo fermi-operator expansion for fractional occupation,” *Journal of Chemical Theory and Computation* **15**, 190–200 (2019).
- ¹²A. M. N. Niklasson, “A note on the pulay force at finite electronic temperatures,” *The Journal of Chemical Physics* **129**, 244107 (2008).
- ¹³A. Marek, V. Blum, R. Johanni, V. Havu, B. Lang, T. Auckenthaler, A. Heinicke, H.-J. Bungartz, and H. Lederer, “The elpa library: Scalable parallel eigenvalue solutions for electronic structure theory and computational science,” *Journal of Physics: Condensed Matter* **26**, 213201 (2014).
- ¹⁴A. Weiße, G. Wellein, A. Alvermann, and H. Fehske, “The kernel polynomial method,” *Rev. Mod. Phys.* **78**, 275–306 (2006).
- ¹⁵R. Zeller, J. Deutz, and P. Dederichs, “Application of complex energy integration to selfconsistent electronic structure calculations,” *Solid State Communications* **44**, 993–997 (1982).
- ¹⁶S. Goedecker, “Linear scaling electronic structure methods,” *Rev. Mod. Phys.* **71**, 1085–1123 (1999).
- ¹⁷M. Gates, J. Kurzak, A. Charara, A. YarKhan, and J. Dongarra, “Slate: Design of a modern distributed and accelerated linear algebra library,” in *Proc. of the International Conference for High Performance Computing, Networking, Storage and Analysis* (2019).
- ¹⁸G. Kwasniewski, M. Kabić, M. Besta, J. VandeVondele, R. Solcà, and T. Hoeftler, “Red-blue pebbling revisited: Near optimal parallel matrix-matrix multiplication,” in *Proc. of the International Conference for High Performance Computing, Networking, Storage and Analysis* (2019).
- ¹⁹NVIDIA, “Cuda math library early access program,” .
- ²⁰P. Motamarri, M. Nowak, K. Leiter, J. Knap, and V. Gavini, “Higher-order adaptive finite-element methods for kohn–sham density functional theory,” *Journal of Computational Physics* **253**, 308–343 (2013).
- ²¹P. Motamarri and V. Gavini, “Subquadratic-scaling subspace projection method for large-scale kohn-sham density functional theory calculations using spectral finite-element discretization,” *Physical Review B* **90** (2014).
- ²²R. McWeeny, “Some recent advances in density matrix theory,” *Rev. Mod. Phys.* **32**, 335–369 (1960).
- ²³A. H. R. Palser and D. E. Manolopoulos, “Canonical purification of the density matrix in electronic-structure theory,” *Phys. Rev. B* **58**, 12704–12711 (1998).
- ²⁴T. Ozaki, “Continued fraction representation of the fermi-dirac function for large-scale electronic structure calculations,” *Phys. Rev. B* **75**, 035123 (2007).
- ²⁵K. Németh and G. E. Scuseria, “Linear scaling density matrix search based on sign matrices,” *The Journal of Chemical Physics* **113**, 6035–6041 (2000).
- ²⁶A. Holas, “Transforms for idempotency purification of density matrices in linear-scaling electronic-structure calculations,” *Chemical Physics Letters* **340**, 552–558 (2001).
- ²⁷A. M. N. Niklasson, “Implicit purification for temperature-dependent density matrices,” *Phys. Rev. B* **68**, 233104 (2003).
- ²⁸D. K. Jordan and D. A. Mazziotti, “Comparison of two genres for linear scaling in density functional theory: Purification and density matrix minimization methods,” *The Journal of Chemical Physics* **122**, 084114 (2005).
- ²⁹E. Rudberg and E. H. Rubensson, “Assessment of density matrix methods for linear scaling electronic structure calculations,” *Journal of Physics: Condensed Matter* **23**, 075502 (2011).
- ³⁰P. Suryanarayana, “Optimized purification for density matrix calculation,” *Chemical Physics Letters* **555**, 291–295 (2013).
- ³¹E. H. Rubensson and A. M. N. Niklasson, “Interior eigenvalues from density matrix expansions in quantum mechanical molecular dynamics,” *SIAM Journal on Scientific Computing* **36**, B147–B170 (2014).
- ³²D. Bowler and M. Gillan, “Density matrices in o(n) electronic structure calculations: theory and applications,” *Computer Physics Communications* **120**, 95–108 (1999).
- ³³L. A. Truffandier, R. M. Dianzinga, and D. R. Bowler, “Communication: Generalized canonical purification for density matrix minimization,” *The Journal of Chemical Physics* **144**, 091102 (2016).
- ³⁴R. K. Gupta and S. D. Senturia, “Pull-in time dynamics as a measure of absolute pressure,” in *Proc. IEEE International Workshop on Microelectromechanical Systems (MEMS’97)* (Nagoya, Japan, 1997) pp. 290–294.
- ³⁵B. D. Cullity, *Introduction to Magnetic Materials* (Addison-Wesley, Reading, MA, 1972).
- ³⁶E. H. Rubensson, “Nonmonotonic recursive polynomial expansions for linear scaling calculation of the density matrix,” *Journal of Chemical Theory and Computation* **7**, 1233–1236 (2011).
- ³⁷M. Methfessel and A. T. Paxton, “High-precision sampling for brillouin-zone integration in metals,” *Phys. Rev. B* **40**, 3616–3621 (1989).
- ³⁸A. M. N. Niklasson, M. J. Cawkwell, E. H. Rubensson, and E. Rudberg, “Canonical density matrix perturbation theory,” *Phys. Rev. E* **92**, 063301 (2015).
- ³⁹M. Wegmuller, J. P. von der Weid, P. Oberson, and N. Gisin, “High resolution fiber distributed measurements with coherent OFDR,” in *Proc. ECOC’00* (2000) p. 109.
- ⁴⁰cuBLAS Library, .
- ⁴¹cuSOLVER Library, .